CHAPTER 24

Fluorescence Lifetime Imaging Microscopy

Ching-Wei Chang, Dhruv Sud, and Mary-Ann Mycek

Department of Biomedical Engineering, University of Michigan
Ann Arbor, Michigan 48109

I. Introduction

There has been significant growth in the use of fluorescence in the biological sciences during the past two decades. Besides environmental monitoring, clinical chemistry, DNA sequencing, and genetic analysis by fluorescence *in situ* hybridization (FISH), fluorescence is used for cell identification and sorting in flow

METHODS IN CELL BIOLOGY, VOL. 81

0091-679X/07 $35.00
DOI: 10.1016/S0091-679X(06)81024-1

cytometry, and to reveal the localization and movement of intracellular substances in cellular imaging by means of fluorescence microscopy (Lakowicz, 1999).

Steady state fluorescence microscopy is routinely employed for studies in cell biology to reveal information regarding cellular morphology, intracellular ion concentrations, protein binding, lipid content, and membrane status (Rudolph and Kempe, 1997). However, it is sensitive to some intensity-based artifacts such as variation in excitation source intensity, detector gain setting, optical loss in the optical path or sample, variation in sample fluorophore concentration, photobleaching, and microscope focusing. Further, fluorophores with similar excitation and emission spectra may be impossible to differentiate in steady state intensity imaging.

Fluorescence lifetime imaging microscopy (FLIM) produces spatially resolved images of fluorophore lifetime (the property describing how rapidly fluorescence decays), providing another dimension of information for visualizing fluorophores and an additional source of contrast. As an example, flavin adenine dinucleotide (FAD) can be distinguished from flavin mononucleotide (FMN) in lifetime imaging, so can ATTO 565 from Rhodamine B (Table I), regardless of the fact that their spectra overlap. Further, lifetimes are known to be sensitive to the fluorophore's

Table I
Endogenous and Exogenous Fluorophores Used in Cell Biology (ISS; Urayama and Mycek, 2003)

Fluorophore	Solvent	Excitation max (nm)	Emission max (nm)	Lifetime (ns)
Endogenous				
Tryptophan	Water	295	353	3.1
Tyrosine	Water	275	304	3.6
Phenylalanine	Water	260	282	6.8
NAD(P)H	Water	350	460	0.4
FAD	Water	450	525	4.7
FMN	Water	450	525	2.3
Exogenous				
ATTO 565	Water	561	585	3.4
Rhodamine B	Water	562	583	1.68
Cy3	PBS	548	562	0.3
Cy5	PBS	646	664	1
DAPI	TRIS/EDTA	341	496	0.16
FITC	PB pH 7.8	494	518	4.1
Fluorescein	PB pH 7.5	495	517	4
GFP	Buffer pH 8	498	516	3.2
Hoechst 33342	TRIS/EDTA	336	471	0.35
Lucifer Yellow	Water	428	535	5.7

PBS, phosphate buffered saline pH 7.4; TRIS/EDTA (1 mM, pH 7.4), tris(hydroxymethyl)aminomethane/ethylenediamine-tetraacetic acid; PB, phosphate buffer.

local environment, while being generally independent of factors influencing fluorescence intensity (Lakowicz, 1999; Tadrous, 2000). For example, Fig. 1 illustrates the capability of FRET-FLIM to detect localization of phosphorylated biomolecules in a cell. Fluorescence resonant energy transfer (FRET) (see Section IV for details) took place when protein kinase Cα (PKCα) molecules were immuno-stained with both Cy3 (donor) and Cy5 (acceptor), which occurred only on phosphorylated PKCα molecules and was indicated by a reduction of donor fluorescence lifetime (Ng *et al.*, 1999). Also note that in Fig. 1, Cy3 was in a different environment from that described in Table I, which explains the lifetime difference and provides another example of the sensitivity of lifetime to its local environment.

Section II will begin with the basics of fluorophore lifetime, including the characteristics of fluorophore decay, a discussion of factors affecting fluorescence lifetimes, and the usefulness of lifetimes as a source for contrast. In Section III, approaches to measuring τ and creating lifetime maps will be discussed. Both time-domain (TD) and frequency-domain (FD) approaches (including data analysis) will be described along with an introduction to different microscopy methods for lifetime imaging. Various applications of FLIM, ranging from commonly used FRET-FLIM to FCS-, MS-MP-, and video-rate FLIM, will be highlighted in Section IV, followed by a summary in Section V.

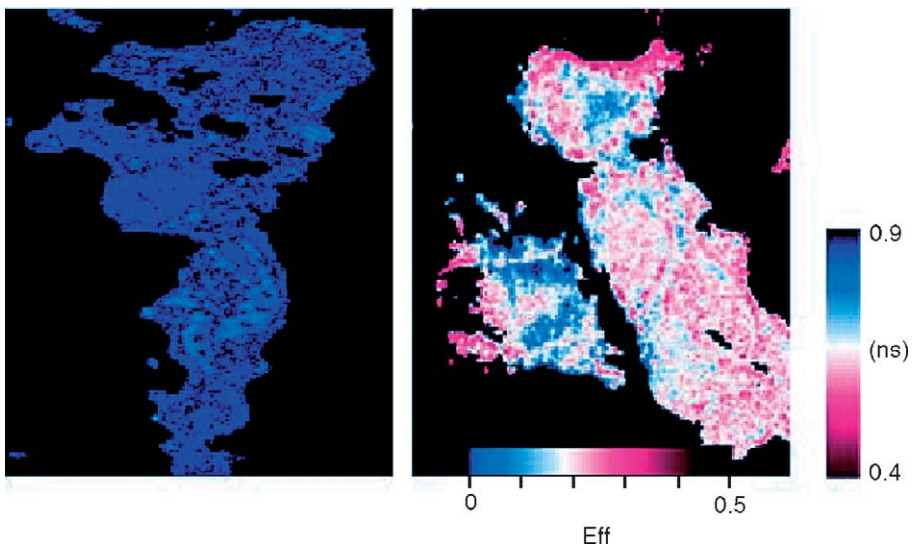

Fig. 1 Individual PKCα molecules were stained either with donor (Cy3) only (left panel) or with donor and acceptor (Cy5) (right panel). FRET from Cy3 to Cy5 took place on individual PKCα molecules that were phosphorylated after tetradecanoyl phorbol acetate (TPA) stimulation in fixed 293T cells, resulting in a reduction of the fluorescence emission lifetime of Cy3 as demonstrated by changes in τ measured in frequency domain. Acceptor labeling was through an antibody specific for the phosphorylated form of PKCα. Eff, energy transfer efficiency [Eq. (42)] (Ng *et al.*, 1999). Reprinted with permission from Ng *et al.* (1999). Copyright 1999 AAAS.

II. Fluorophore Excited State Lifetime: τ

A. Basic Theory

Figure 2 is a simplified version of a Jablonski diagram to illustrate the fluorescence process, where S_0 and S_1 are the ground and first excited electronic states, respectively, and the horizontal lines represent different vibrational states of the fluorophore. In condensed phases, after light absorption, almost all molecules rapidly relax to the lowest vibrational state of the first excited state, from which molecules return to the ground state via one of two decay processes: nonradiative (k) or radiative (Γ) decay. The radiative decay rate Γ depends on the electronic properties of an isolated fluorophore. Molecular interactions, such as dynamic (or collisional) quenching and energy transfer, are treated in the nonradiative decay rate k. Radiative decay is responsible for fluorescence emission, providing detectable photons. However, since both decays depopulate fluorescent molecules in first excited state, with population $N(t)$, the decay of fluorescence emission intensity, proportional to $N(t)$, is attributed to both decay rates, and, in the most simple case, follows the stochastic hence exponential decay as shown in Eqs. (1) and (2).

$$\frac{\mathrm{d}N(t)}{\mathrm{d}t} = -(\Gamma + k)N(t) \tag{1}$$

$$N(t) = N_0 \mathrm{e}^{-(\Gamma+k)t} = N_0 \mathrm{e}^{-t/\tau} \tag{2}$$

where N_0 is the initial number of fluorescent molecules in the first excited state, and

$$\tau = \frac{1}{\Gamma + k} \tag{3}$$

is the fluorescence lifetime, reflecting the average time a molecule spends in the excited state prior to return to the ground state. As is evident, both nonradiative

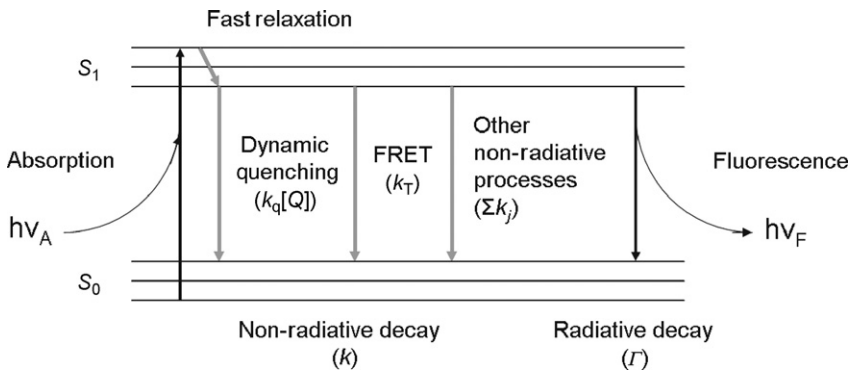

Fig. 2 Simplified Jablonski diagram. k_q, bimolecular quenching constant; [Q], quencher concentration (Section II.B); k_T, energy transfer rate constant (Section IV.A); k_j, rate constant for nonradiative processes other than dynamic quenching and FRET.

and radiative decays play a role in the value of τ, and hence in the fluorescence emission process. Another important property of fluorophores is quantum yield, defined as the ratio of the number of emitted photons to the number of absorbed photons, which is given by

$$Q = \frac{\Gamma}{\Gamma + k} \tag{4}$$

Note that $0 \leq Q \leq 1$ and Q can be close to unity if $k \ll \Gamma$. Generally, higher quantum yield means brighter fluorescence signals, which is usually favored in fluorescence applications. Although Q can be used as a source of contrast, experimental protocols for estimating Q are strict and controlled, making it difficult to apply in biological samples.

B. Key Features of Lifetime Sensing

Fluorescence lifetime is an intrinsic property of fluorophores and is insensitive to intensity artifacts such as variation in excitation source intensity, detection gain setting, optical loss in the optical path or sample, variation in sample fluorophore concentration, photobleaching, and microscope focusing. Figure 3 is an illustration of intensity-independence of lifetime imaging. Despite the fact that fluorescence intensity revealed the fluorophore concentration difference between samples, no significant lifetime differences were observed, reflecting the insensitivity of lifetime to intensity artifacts. On the other hand, due to the nature of the nonradiative decay process, lifetimes are sensitive to the fluorophore's microenvironment, including factors such as temperature, pH, oxygen concentration, polarity, molecular associations (binding), ion concentration, and relaxation through collisional (dynamic) quenching and FRET.

The concepts of static and dynamic quenching are shown in Fig. 4. Static quenching occurs due to the formation of nonfluorescent complexes from the interaction between fluorophores and other molecules in solution known as quenchers. Lifetime imaging is insensitive to static quenching, since unbound fluorophores retain their fluorescence properties. On the other hand, dynamic quenching happens during the decay process, when excited state fluorophores are deactivated on contact with the quenchers. As a result, these quenched fluorophores will follow nonradiative decay process (Fig. 2), which leads to a quicker decay of fluorescence and hence a shorter lifetime.

Therefore, lifetime measurement provides a means of probing the local fluorophore environment. FLIM was reported (Sanders *et al.*, 1995) for quantitative pH determination in living cells with the fluorescent probe c.SNAFL-1. It was found that a lifetime-based approach was easier to employ than traditional ratiometric technique, while still providing accurate information regarding intracellular pH. Another FLIM-based pH measurement was presented in (Lin *et al.*, 2003), which suggested that FLIM can measure the intracellular pH of the resting cells and follow the pH fluctuations inside the cells after environmental perturbations.

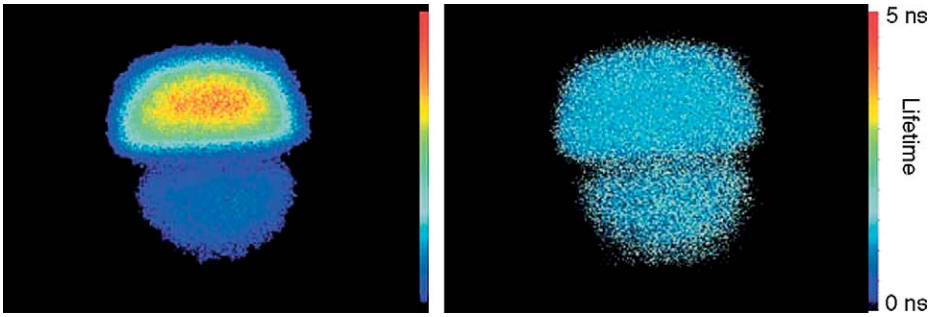

Fig. 3 Intensity-independent fluorophore lifetimes recovered by FLIM. Despite a factor of four difference in POPOP concentration and hence signal intensity (left), the three-gate protocol lifetime map (right) showed identical mean lifetimes for the two POPOP samples. The images were of POPOP in ethanol solutions in two quartz capillaries. The capillary interface was on the diameter, with the circular region as the illumination area. The intensity images were background subtracted before calculation of lifetime map (Urayama *et al.*, 2003). With kind permission of Springer Science and Business Media.

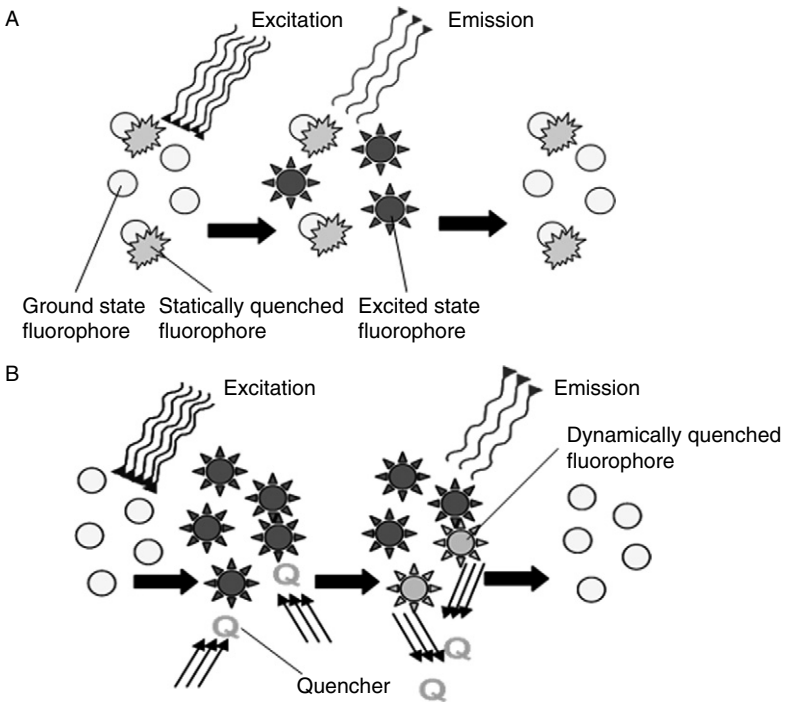

Fig. 4 Static quenching (A) occurs due to the formation of nonfluorescent complexes from the interaction between fluorophores and other molecules in solution known as quenchers. Lifetime imaging is insensitive to static quenching. On the other hand, dynamic quenching (B) happens during the decay process, when excited state fluorophores are deactivated on contact with the quenchers. As a result, detected lifetime will be shortened.

Measurement of dissolved oxygen concentration in single living cells was demonstrated by Sud *et al.* (2006) and Gerritsen *et al.* (1997) (Fig. 5). Because the probe's fluorescence emission was found to be dynamically quenched by oxygen, the probe's lifetime was directly dependent on local oxygen concentration and could be used for quantitative imaging in cells via FLIM (Urayama and Mycek, 2003a). Molecular interactions such as binding of the endogenous fluorophore nicotinamide adenine dinucleotide (NADH) to malate dehydrogenase have been imaged with FLIM (Lakowicz *et al.*, 1992), by using the increase in NADH lifetime on binding as a source of contrast. NADH lifetime increased by ~150% and was much easier to detect than the blueshift of the emission spectrum that was only ~20% of the full width at half-maximum (FWHM) in fluorescence intensity measurement. Finally, FRET between the phospholipids NBD-PE (energy donor) and LRB-PE (energy acceptor) was employed to monitor endosomal fusion in single living cells (Oida *et al.*, 1993). FRET involves nonradiative energy transfer between fluorophores, and will be discussed in detail in Section IV.A. Excellent reviews providing further historical FLIM background can be found in (French *et al.*, 1998; Gadella, 1999; Tadrous, 2000; Wang *et al.*, 1992).

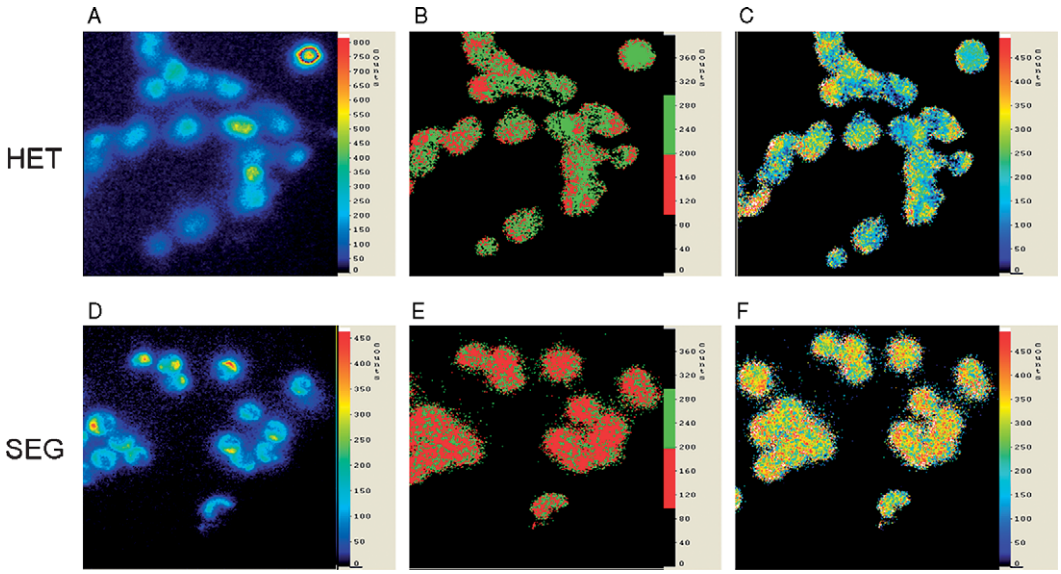

Fig. 5 RTDP fluorescence intensity (A and D), lifetime in nanoseconds (B and E), and oxygen in micromolars (C and F) maps of normal human squamous esophageal epithelial cells (HET) (A–C) and Barrett's adenocarcinoma esophageal cells (SEG) (D–F). The intensity images (A and D) could not be reliably used to discriminate between the two different cell lines. The binary lifetime maps (B and E), on the other hand, plainly indicate different lifetimes for these two cellular species, with the SEG recording lower lifetimes than the HET. For the given case, $\tau_{HET} = 225$ ns and $\tau_{SEG} = 170$ ns. The mean lifetime difference was found to be $\Delta\tau = 44 \pm 7.48$ ns. Logically, this translated into higher oxygen levels in the SEG versus the HET using the calibration derived, as can be seen in the oxygen distribution maps (C and F) (Sud *et al.*, 2006).

III. Methods for Creating Intracellular Lifetime Maps

A. Basic TD and FD Approaches

The objective of both TD and FD measurements is to recover the lifetime parameter that describes fluorescence decay, which provides additional information that is lost during steady state intensity measurements. Both TD and FD methods (equivalent and related by the Fourier transform) have comparable temporal resolution and discrimination, and benefit from continual evolution of imaging technologies. The choice of FLIM instrumentation hence depends on the particular application: FD FLIM is better suited for evaluating multiexponential decays, while TD FLIM is optimal for flexible, large temporal range systems and especially apt for long-lifetime measurements.

Measuring lifetime (τ) via TD is more intuitive. It exploits the fact that the fluorescence emission is theoretically proportional to the number of molecules in the first excited state, and hence it decays exponentially, as described in Section II.A. The exponential decay can be reconstructed in different ways, most commonly used of which are gated integration and time-correlated single photon counting (TCSPC), which will be described in detail in Section III.C.

Figure 6 illustrates the instrumentation and concepts of gated integration TD approach to measuring lifetime τ. A mode-locked or cavity-dumped laser, or a discharge source, is typically used to provide pulse excitation. The pulse is split by a beam-splitter into two paths, one of which excites the sample on the microscope

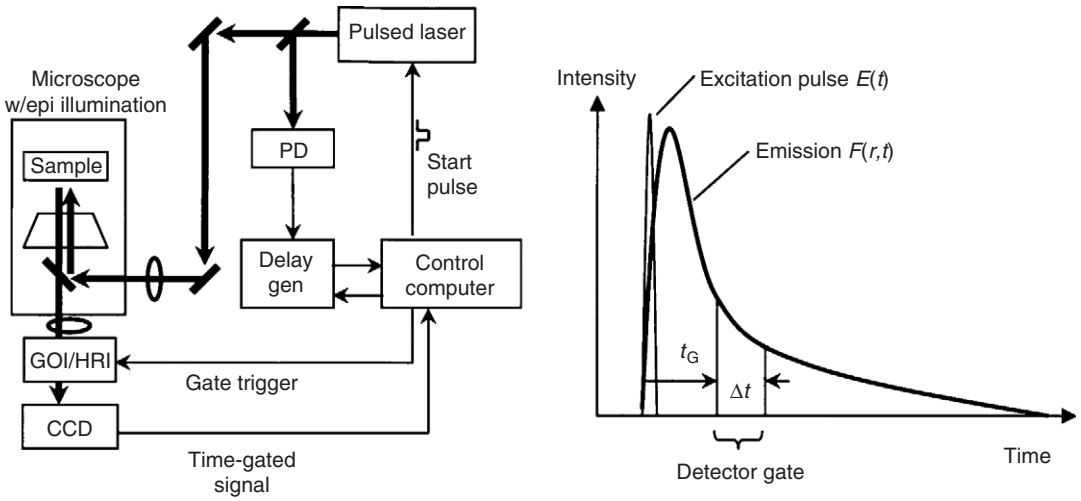

Fig. 6 Time-domain lifetime imaging instrumentation and concepts (Urayama and Mycek, 2003). The variable *r* indicates parameters that are spatially varying. Abbreviations for instrument schematics: PD, photodiode; delay gen, delay generator; GOI, gated optical intensifier; HRI, high rate imager; CCD, charge coupled device (camera); thick solid lines, light path; thin solid line, electronic path.

stage, while the other triggers the gated charge-coupled device (CCD) camera, with programmable delays. After sample excitation, the fluorescence emission is collected by the CCD. During the time period the CCD gate is open, the received fluorescence signal is integrated (a convolution with the gated detector gain). Gates with different delays provide different regions of the recorded signal waveform, making it possible to reconstruct the exponential decay curve.

The basic principle of FD FLIM is illustrated in Fig. 7 for a wide-field system, though this approach is readily applicable to confocal systems (Fig. 8) (Booth and Wilson, 2004). A sinusoidally modulated light source is used for excitation. The resulting sample emission is also sinusoidally modulated at the same frequency as the excitation, but is shifted in phase and is demodulated to some extent, i.e. has a reduced modulation depth. Fluorescence lifetime can be directly calculated by changes in phase delay and demodulation. For measuring different lifetimes, different modulating frequencies need to be used. Note that measured phase delay between excitation and emission is in the range 0–90°, although arbitrarily long delays (>90°) can be introduced by optical delay lines. Demodulation of the emission is measured as a factor $M(x)$ (Fig. 6), which has a value of 0–1. It is logical that at low frequencies, emission from samples with low lifetimes (fast decays) will follow the excitation faithfully; hence the phase delay will be nearly 0° and the demodulation nearly 1. As the modulation frequency is increased, the finite lifetime of the fluorophore prevents this and is reflected in a phase delay

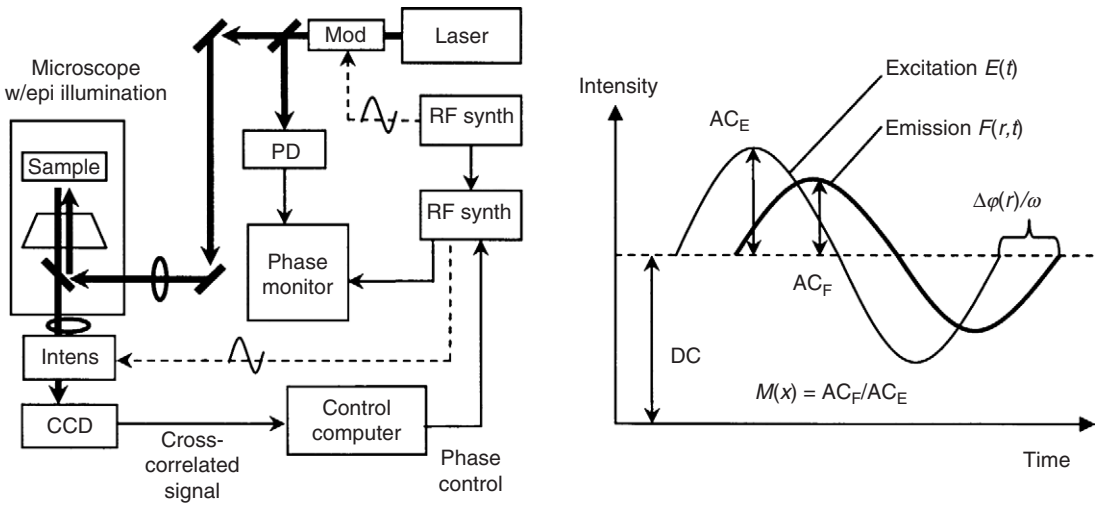

Fig. 7 Frequency-domain lifetime imaging instrumentation and concepts (Urayama and Mycek, 2003). The variable *r* indicates parameters that are spatially varying. Abbreviations for instrument schematics: PD, photodiode; CCD, charge coupled device (camera); RF synth, RF synthesizer; mod, intensity modulator; thick solid lines, light path; thin solid line, electronic path; dashed line, RF signal path.

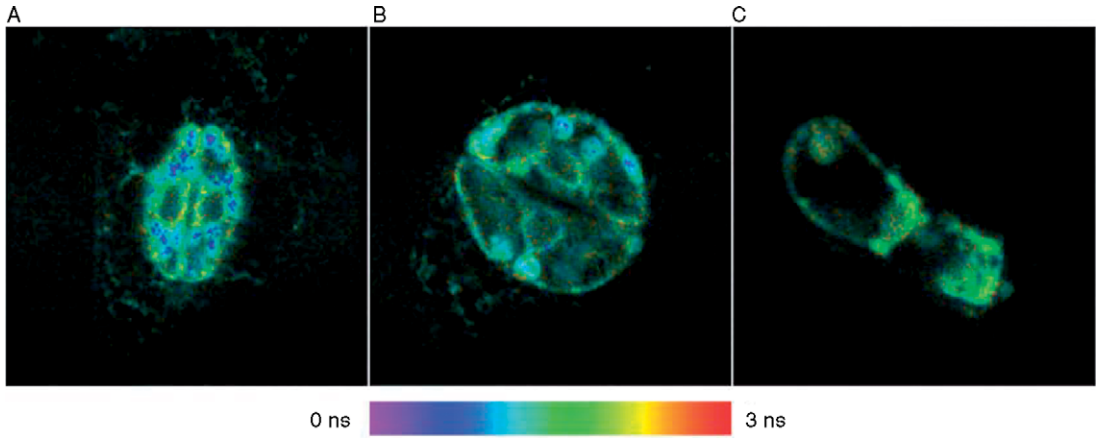

Fig. 8 Combined fluorescence intensity and phase lifetime images of *Nicotiana tabacum* specimens with a confocal system. The fluorescence is a combination of autofluorescence and GFP fluorescence. (A and B) Stomata of leaves in which the endoplasmic reticulum was labeled with GFP5. (C) A trichrome of a leaf with GFP5-labeled Golgi. The hue of the images represents the fluorescence lifetime corresponding to the scale shown from 0 to 3 ns. The image widths are: (A) 100 μm, (B) 70 μm, and (C) 65 μm (Booth and Wilson, 2004). Copyright 2004 Blackwell Publishing.

as well as demodulation of the emission. At extremely high excitation frequencies, phase delay will be 90° while demodulation will be 0.

The phase angle and demodulation, plotted over a range of frequencies, provide the frequency response of the sample. Typically, the plot is limited to a "useful frequency" range in which changes in phase and demodulation are frequency dependent. As a general rule, the center frequency of this plot is approximately the reciprocal of the lifetime. Hence, typical biological fluorophores such as NAD(P)H and collagen with lifetimes of few nanoseconds need excitation sources modulated at 1–200 MHz. Long-lived fluorophores such as platinum and ruthenium-ligand complexes have lifetimes of microseconds and hence the modulation is tens of kHz to 1 MHz. Measurement of lifetimes in the low picosecond range (e.g., Rose Bengal, 90ps) requires modulated sources at frequencies of ~2 GHz.

A detailed treatment of standard FD FLIM instrumentation and its variants can be found elsewhere (Lakowicz, 1999). Briefly, radio frequency modulation (MHz range) of a light source is done via acousto- or electro-optic modulators. The light source can be CW (argon-ion laser, arc lamps) or even a high repetition rate pulsed laser. On the detection side, cross-correlation is used to extract low-frequency phase and demodulation information by modulating the detector at a frequency offset from the modulation frequency, a scheme known as heterodyne detection (see data analysis). For sync operation, the same RF synthesizer is hence used for modulating the light source as well as providing the reference signal for the intensifier on the CCD.

B. Microscopy Systems Compatible with Lifetime Imaging

Depending on the mechanism of illumination and detection, microscopes can be classified into wide-field, confocal, and multiphoton systems, on each of which lifetime imaging can be implemented. Wide-field microscopy illuminates the entire specimen to provide single-shot image acquisition. When used in fluorescence microscopy, it is rapid but has limited spatial resolution, since the fluorescence emitted from above and below the focal plane is also captured in the image and interferes with the resolution of in-focus features.

Confocal microscopy is a point-scanning approach which circumvents this artifact by filtering out defocused light from the object with a pinhole located in front of the image plane. Because only the light within the focal plane is allowed through the pinhole, it offers higher spatial and axial resolution, therefore revealing more detail in the specimen. However, since much light is eliminated by the pinhole, reducing the final image intensity and hence signal-to-noise ratio (SNR), high-energy lasers and highly sensitive photomultiplier tubes (PMTs) are needed for each point in the specimen and scanning through all the points of interest is required.

Multiphoton microscopy utilizes more than one photon to excite the sample. Each photon, with a longer wavelength than that of the absorption peak of the fluorophore (e.g., two-fold wavelength for two-photon microscopy), has only one part of the required energy to excite the fluorophore to the first excited state. Since multiphoton excitation requires high photon density, probability of multiphoton excitation exists mostly at the focal point. Since the excitation source is not attenuated by absorption by fluorophore above the focal plane, and less scattering occurs for longer excitation wavelengths, optical sections may be obtained from deeper within a tissue by using multiphoton microscopy.

All microscopy systems described above are extensible for lifetime imaging. The best approach depends on the requirements of the sample.

C. Time-Domain FLIM

Following the instrumentation setup in Fig. 6, described in Section III.A, the resulting fluorescence is a convolution of the sample's intrinsic fluorescence decay with the excitation profile (the instrument response function, IRF) $E(t)$. For a sample with a spatially dependent, j-component multiexponential lifetime, the fluorescence signal $F(r, t)$ is therefore

$$\begin{aligned} F(r,t) &= E(t) \otimes \sum_j \alpha_j(r) \mathrm{e}^{-(t/\tau_j(r))} \\ &= \int_{-\infty}^{t} E(t') \sum_j \alpha_j(r) \mathrm{e}^{-((t-t')/\tau_j(r))} \mathrm{d}t', \end{aligned} \tag{5}$$

where $\tau_j(r)$ and $\alpha_j(r)$ are the lifetime and amplitude of the jth component, respectively. The variable r emphasizes the spatial dependence of the fluorescence lifetime such as a pixel location on an area detector. $E(t)$ is determined using a reference with very

short lifetime so that the decay is effectively a delta function. With $E(t)$ known, the lifetime $\tau_j(r)$ is fit to measured decays by using deconvolution algorithms such as least squares iterative reconvolution (Urayama and Mycek, 2003a).

Because $F(r, t)$ detection must preserve both spatial and temporal information, a gated intensified CCD (ICCD) camera is often used. The fluorescence is imaged during a short interval $G(t)$ representing the gated detector gain, which can be described with a rise time t_R, fall time t_F, and gate width Δt. For a gate opening at time t_G, the detected image $D(r, t_G)$ is given by

$$D(r, t_G) = \int_{-\infty}^{\infty} G(t' - t_G)F(r, t')\mathrm{d}t'. \tag{6}$$

The temporally and spatially resolved decay of the sample fluorescence is then reconstructed by acquiring images at different t_G, which is synchronized to the excitation pulse by using a photodiode coupled with electronics capable of variable delays.

Because it requires a well-sampled signal profile and can be computationally intensive, deconvolution in TD FLIM using iterative algorithms may not be practical. Instead, picosecond and femtosecond sources, which can be regarded as delta excitations, are employed to eliminate the need for $E(t)$ deconvolution because fluorophore lifetimes are in the 0.1–10 ns regime. Also, the effects of $G(t)$ convolution can be removed by using ratios of detected intensities (described below), or recently available ICCD's with gate widths as fast as tens of picoseconds (Dowling *et al.*, 1997), so that $G(t)$ deconvolution may not be necessary (Urayama and Mycek, 2003a).

For rapid lifetime image acquisition, an analytic rapid lifetime determination (RLD) algorithm can be used (Bugiel *et al.*, 1989; Sharman *et al.*, 1999; Wang *et al.*, 1991). As an example of how using intensity ratios eliminates gate parameters, and also an example of analytic lifetime determination, consider a sample with a single exponential lifetime excited by a negligibly short excitation pulse. For an effective gate width Δt, the gated detector signal at time t is

$$D(r, t) = \int_{t}^{t+\Delta t} \alpha \mathrm{e}^{-(t'/\tau(r))}\mathrm{d}t' = \alpha\tau[\mathrm{e}^{-(t/\tau(r))} - \mathrm{e}^{-((t+\Delta t)/\tau(r))}]. \tag{7}$$

A spatially resolved lifetime $\tau(r)$ can be determined by using two images gated at times t_1 and t_2 (Wang *et al.*, 1992) so that

$$\tau(r) = \frac{t_2 - t_1}{\ln(D(r, t_1)/D(r, t_2))}, \tag{8}$$

where the gate width cancels from the ratio. Because the lifetime determination is analytic and requires only two gates, a 2D image of lifetimes can be constructed rapidly. The acquisition of only two gates allows one to measure the lifetime map in real time, since image acquisition and processing take a fraction of a second (Cubeddu *et al.*, 2002). In practice, a two-gate scheme can be sensitive to noise,

therefore methods using N gates (N typically equal to 5–10) (Cubeddu *et al.*, 2002) can be used with least squares method to increase data redundancy and give more stable results. In this case, lifetime images were calculated on a pixel-by-pixel basis by fitting the lifetime of pixel p (t_p) in image i to the logarithm of the intensity as follows:

$$\ln I_{i,p} = -\frac{t_i}{t_p} + C, \tag{9}$$

where $I_{i,p}$ is the intensity of pixel p in image i, t_i is the gate delay of image i, and C is a constant. Analytic least squares lifetime fits were:

$$\tau_p = -\frac{N\left(\sum t_i^2\right) - \left(\sum t_i\right)^2}{N\sum t_i \ln I_{i,p} - \left(\sum t_i\right)\left(\sum \ln I_{i,p}\right)}, \tag{10}$$

where N is the number of images. All sums are over i.

For more complicated fluorescence decays, double exponential (Cubeddu *et al.*, 2002; Sharman *et al.*, 1999) and nonexponential decays (Lee *et al.*, 2001) have been considered.

In addition to gated detection, TCSPC has also been implemented in TD FLIM (Becker *et al.*, 2002; Böhmer *et al.*, 2001; Bugiel *et al.*, 1989; Ghiggino *et al.*, 1992). Figure 9 clearly demonstrates the concepts of TCSPC. The sample is repetitively excited using a pulse light source, and after each excitation, the first emitted photon is recorded. Since the exponential emission decay curve follows the shape of $N(t)$, which is proportional to the probability density that a photon is emitted at time t, the decay signal waveform can be reconstructed by counting the first photons emitted at time t (or, actually in series of intervals, or channels, of time). In practice, time-correlated memory locations are used to record the counts of the first photons such that a time-correlated histogram can be constructed. TCSPC can be very precise since the accuracy of the time measurement is not limited by the width of the detector pulse.

In terms of instrumentation (Lakowicz, 1999), a PMT is used to monitor each excitation pulse in order to produce a start signal to trigger the voltage ramp of a time-to-amplitude converter (TAC), which will be stopped on detection of first emitted photon, providing an output pulse whose voltage is proportional to the time between the start and stop signals. A multichannel analyzer (MCA) converts this voltage to a time channel using an analog-to-digital converter (ADC). According to different time channels (memory locations) where the photons are recorded, a probability histogram of counts is constructed versus time channels, from which the waveform of exponential decay is revealed.

An alternative is reversed start–stop scheme in which TAC is activated and starts building up voltage when receiving the first photon. The voltage increase is stopped when a signal pulse is received, which can be either the pulse from the next period, or, if considering possible jitter of the pulses, delayed pulse from the same period (the pulse that actually excited the photon). The reversal of time axis in the

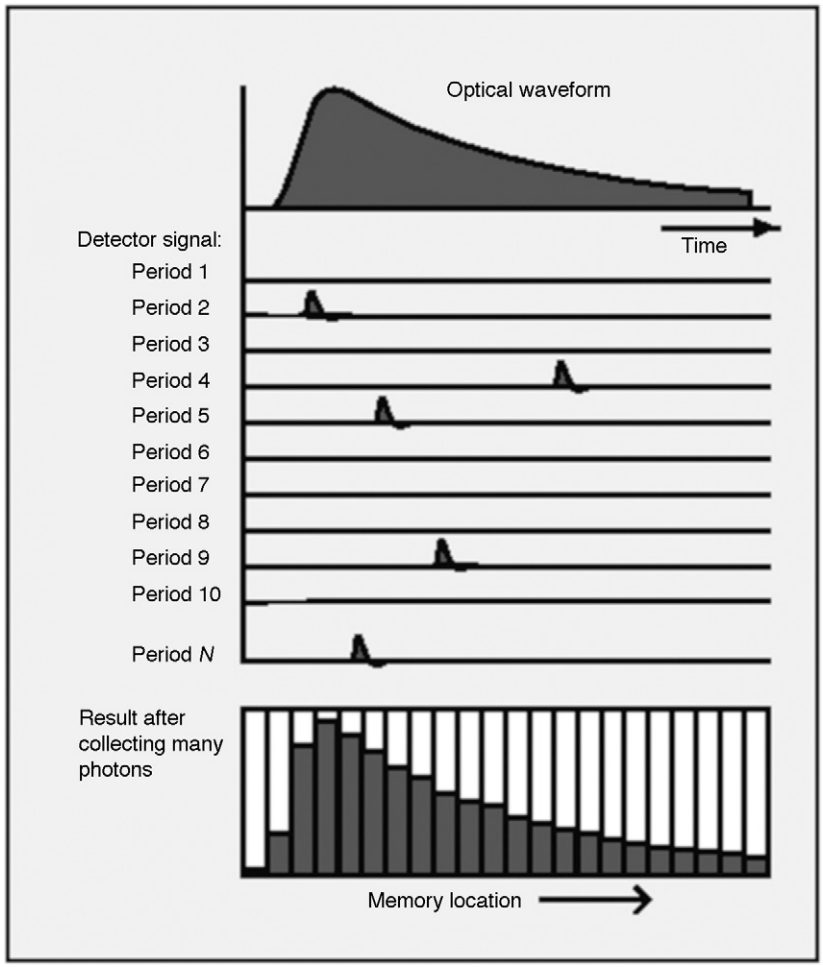

Fig. 9 Concepts of time-correlated single photon counting (TCSPC) (Becker and Bergmann, 2003). The sample is repetitively excited using a pulse light source, and after each excitation, the first emitted photon is recorded. By counting the first photons emitted at time t, $N(t)$ can be reconstructed. In practice, time-correlated memory locations are used to record the counts of the first photons such that a time-correlated histogram can be constructed.

final data can be easily compensated for electronically. The advantage of reversed start–stop is that TAC does not have to be constantly activated and reset in every pulse period, considering the fact that in most pulse periods actually no photon is recorded. However, reversed start–stop may cause some sort of counting loss distortion (explained below).

In fact, the photon counting rate is usually set to be only ~1% to avoid pileup effect (one kind of counting loss effects), which distorts the TCSPC data to the

earlier times and makes the decay look faster than it really is, since the photons detected after receiving the first photon, if any, will not be recorded. Simulations have been done to reveal such effect (Demas, 1983; Salthammer, 1992). The classic pileup effect on a single exponential lifetime and its correction are described below (Becker, 2005).

The probability, P_k, that a photon appears at a time corresponding to channel k in one signal period is

$$P_k = P_0 \mathrm{e}^{-k\Delta t/\tau}, \tag{11}$$

with Δt is the time channel width, P_0 is the probability of a count in the first channel of the fluorescence decay. The sum of the probabilities, P_k, for all time channels is the probability, P, of detecting a photon in one signal period

$$P = \sum_{k=1}^{\infty} P_k = \sum_{k=1}^{\infty} P_0 \mathrm{e}^{-k\Delta t/\tau}. \tag{12}$$

Note that the value of P can be greater than one, which can be interpreted as the average number of detected photons during one signal period. Following the derivation described in (Becker, 2005), the pileup distorted waveform of the recorded signal can be written as

$$f(k) = \mathrm{e}^{-k\Delta t/\tau} + \frac{1}{1!} P \mathrm{e}^{-2k\Delta t/\tau} + \frac{1}{2!} P^2 \mathrm{e}^{-3k\Delta t/\tau} + \frac{1}{3!} P^3 \mathrm{e}^{-4k\Delta t/\tau} + \ldots. \tag{13}$$

By using intensity-coefficient-weighted average

$$\tau_{\mathrm{meanc}} = \frac{\sum a_i \tau_i}{\sum a_i}, \tag{14}$$

where a_i represents coefficients of different exponential terms, the averaged lifetime is

$$\tau_{\mathrm{meanc}} = \frac{\tau + (\tau/2)(1/1!)P + (\tau/3)(1/2!)P^2 + (\tau/4)(1/3!)P^3 + \ldots}{1 + (1/1!)P + (1/2!)P^2 + (1/3!)P^3 + \ldots} \tag{15}$$

If P is small, the approximated value is

$$\tau_{\mathrm{meanc}} \approx \tau\left(1 - \frac{P}{2}\right), \tag{16}$$

which can be used for pileup effect correction. An alternative is to calculate integral-intensity-weighted lifetime

$$\tau_{\mathrm{meani}} = \frac{\sum a_i \tau_i^2}{\sum a_i \tau_i}, \tag{17}$$

which leads to

$$\tau_{\text{meani}} = \tau \frac{1 + (1/2)(1/2!)P + (1/3)(1/3!)P^2 + (1/4)(1/4!)P^3 + \ldots}{1 + (1/2!)P + (1/3!)P^2 + (1/4!)P^3 + \ldots}. \tag{18}$$

With small P, we have

$$\tau_{\text{meani}} \approx \tau\left(1 - \frac{P}{4}\right). \tag{19}$$

One feature of TCSPC is that almost all detected photons contribute to the result of the measurement, and there is no loss due to "gating" as in gated image intensified CCDs. Counting loss occurs when there is classic pileup effect as described above, or when system has a dead time in which any detected photons cannot be recorded. The recorded count rate, r_{rec}, can be expressed as

$$r_{\text{rec}} = \frac{r_{\text{det}}}{1 + r_{\text{det}} t_{\text{d}}}, \tag{20}$$

where r_{det} is the detector count rate, and t_{d} is the dead time. The counting efficiency can therefore be defined as

$$E = \frac{r_{\text{rec}}}{r_{\text{det}}} = \frac{1}{1 + r_{\text{det}} t_{\text{d}}} \tag{21}$$

In these two equations, continuous light signal is assumed. With pulse signals, dead-time-related distortion may occur when using reversed start–stop scheme, since TAC/ADC dead time may extend into one of the subsequent pulse period. This will favor photon recording in the later part of pulse period, which might counteract the classic pileup effect. In fact, dead-time-related distortion cannot be easily corrected, because the dead time may vary with the TAC voltage, and the blind-to-active transition may cause ripple in the TAC characteristic, too (Becker, 2005).

Data analysis of TCSPC can be performed using several different methods, including nonlinear least squares analysis, the method of moments, Laplace transformation, and the maximum entropy method, and some other methods, but nonlinear least squares method remains to be the most general and reliable method for analysis of time-resolved data (Lakowicz, 1999). The goal of nonlinear least squares method is to minimize goodness of fit (χ^2) by varying the values of model parameters. χ^2 is expressed as

$$\chi^2 = \sum_{k=1}^{n} \frac{1}{\sigma_k^2} [N(t_k) - N_c(t_k)]^2 = \sum_{k=1}^{n} \frac{[N(t_k) - N_c(t_k)]^2}{N(t_k)} \tag{22}$$

where n is the total number of channels, $N(t_k)$ is the observed count number in channel k, $N_c(t_k)$ is the calculated count number in channel k from model prediction,

and σ_k^2 is the variance of $N(t_k)$, which is equal to $N(t_k)$ from Poisson statistics. χ^2 is actually a variance-weighted least squares statistic, which follows statistical chi-square distribution. Since values of the numerator and denominator in Eq. (22) will be close if the model accounts for the data, χ^2 will have a value close to the number of channels, n. In practice, reduced χ^2, χ_R^2, is defined as follows:

$$\chi_R^2 = \frac{\chi^2}{n-p} = \frac{\chi^2}{v} \tag{23}$$

where p is the number of model parameters and v is the degree of freedom. Because n is usually much larger than p, χ_R^2 typically has a value near unity. A table of χ_R^2 distribution, showing the p values for various χ_R^2 values with different degrees of freedom, will help decide how well the model fits the data. Since systematic errors in the data can easily result in a 10–20% elevation of χ_R^2, a model would be acceptable if p value is not statistically significant at 5% significant level. However, when choosing a better model (for simple models vs complex models), relative χ_R^2 values may be more important than absolute χ_R^2 values (Lakowicz, 1999).

The moment method of TCSPC data analysis, or the "centroid shift" method, was used in the early days of TCSPC to calculate fluorescence and excited nuclear state lifetimes from measurement data. It has a benefit that the statistical accuracy of τ can be easily estimated (Becker, 2005).

For the discrete function, count number $N(t_k)$ in channel k, the first moment, or the "centroid," is

$$M_1 = \frac{\sum_{k=1}^{n} N(t_k) t_k}{N} \tag{24}$$

where t_k is the time of channel k and N is the total photon count number in all channels. M_1 can be interpreted as the average photon arrival time and hence is the lifetime of the measured fluorescence. Since two convolved functions have their first moments added linearly, the fluorescence lifetime is

$$\tau = M_{1f} - M_{1IRF} \tag{25}$$

where M_{1f} is the first moment of fluorescence measurement and M_{1IRF} is the first moment of IRF.

D. Frequency-Domain FLIM

One difficulty of FD measurements is accurate estimation of phase angle and modulation at high frequencies. In heterodyne detection, the signal waveform at the modulation frequency F is convolved with a reference waveform at frequency $F + \Delta F$ ($\Delta F = 10$–100 Hz). The slow response of the CCD acts as a low-pass filter that removes the high frequency component in the resulting waveform and provides an easily detectable, slowly varying signal with the phase and modulation information. Another approach known as homodyne detection involves setting $\Delta F = 0$.

The resulting signal (after low-pass filtering) is a static phase-dependent signal. A detailed treatment of FD data analysis can be found in (Urayama and Mycek, 2003a).

Presented below is an outline of a polar plot method for FD analysis of fluorescence lifetimes, which has been reported for single-frequency measurements of samples exhibiting more than one fluorescence lifetime (Redford and Clegg, 2005). The polar plot method is based on well-known procedures used over the years for analysis of dielectric relaxation experiments and has been used as a visual aid for understanding that modulation lifetimes at a single frequency are longer than phase lifetimes for samples exhibiting multiexponential decays.

In FD experiments, excitation light is of the form

$$E(t) = E_0 + E_\omega \cos(\omega t + \phi_E), \tag{26}$$

where ω is the modulation frequency, ϕ_E is the phase of the excitation light and E_0, E_ω are the DC and AC components, respectively. Depth of modulation is defined as $M_E = E_\omega/E_0$. The fluorescence signal can be expressed as

$$S(t) = S_0 + S_\omega \cos(\omega t + \phi_S), \tag{27}$$

For a single exponential system, the relationship between phase, modulation, and lifetime is given by:

$$\phi(\tau) = \arctan(\omega\tau) \tag{28}$$

and

$$M(\tau) = \frac{1}{\sqrt{1 + (\omega\tau)^2}}. \tag{29}$$

From here on, parameters needed for polar plot analysis are provided. For a collection of fluorophores with lifetime, intensity (steady state) is given by:

$$S_0(\tau) = \beta \sum_i c_i(\tau)\varepsilon_i(\tau)Q_i(\tau), \tag{30}$$

where $c_i(\tau)$, $\varepsilon_i(\tau)$, and $Q_i(\tau)$ are the concentration, absorption coefficient, and quantum yield of the ith species with a lifetime τ, respectively, and β is an instrumentation constant such that the summation of $S_0(\tau)$ over all lifetime provides the total intensity, given by $\int_\tau S_0(\tau)\mathrm{d}\tau$. Eq. (27) can be rewritten as

$$\begin{aligned} S_{\mathrm{tot}}(t) &= S_{0\mathrm{tot}} + S_{\omega\mathrm{tot}} \cos(\omega t + \phi_{\mathrm{tot}}) \\ &= \int_\tau (S_0(\tau) + S_\omega(\tau) \cos(\omega\tau + \phi(\tau)))\mathrm{d}\tau \\ &= \int_\tau S_0(\tau)(1 + M(\tau) \cos(\omega\tau + \phi(\tau)))\mathrm{d}\tau. \end{aligned} \tag{31}$$

The $M_{\text{tot}}\cos(\omega\tau + \phi_{\text{tot}})$ term, which represents the time varying part in terms of signal modulation and is equal to the second term in Eq. (31) divided by $S_{0\text{tot}}$, can be broken down as

$$M_{\text{tot}}(\cos\phi_{\text{tot}}\cos\omega t + \sin\phi_{\text{tot}}\sin\omega t) = \int_{\tau}[S_0(\tau)/S_{0\text{tot}}]M(\tau)(\cos\phi(\tau)\cos\omega t + \sin\phi(\tau)\sin\omega t)\mathrm{d}\tau. \tag{32}$$

To yield

$$M_{\text{tot}}\cos\phi_{\text{tot}} = \int_{\tau} I(\tau)M(\tau)\cos\phi(\tau)\mathrm{d}\tau \tag{33}$$

and

$$M_{\text{tot}}\sin\phi_{\text{tot}} = \int_{\tau} I(\tau)M(\tau)\sin\phi(\tau)\mathrm{d}\tau \tag{34}$$

where $I(\tau) = S_0(\tau)/S_{0\text{tot}}$, or the fraction of intensity contributed by fluorophores with lifetime τ. Total phase shift and modulation can now be estimated as:

$$\tan\phi_{\text{tot}} = \frac{\int_{\tau} I(\tau)M(\tau)\sin\phi(\tau)\mathrm{d}\tau}{\int_{\tau} I(\tau)M(\tau)\cos\phi(\tau)\mathrm{d}\tau} \tag{35}$$

$$M_{\text{tot}}^2 = \left(\int_{\tau} I(\tau)M(\tau)\cos\phi(\tau)\mathrm{d}\tau\right)^2 + \left(\int_{\tau} I(\tau)M(\tau)\sin\phi(\tau)\mathrm{d}\tau\right)^2 \tag{36}$$

Nonlinearity of Eqs. (35) and (36) can be changed by using the polar variables

$$x = M(\tau)\cos\phi(\tau) \tag{37}$$

and

$$y = M(\tau)\sin\phi(\tau) \tag{38}$$

On this x–y plot, M is the distance from the origin and ϕ is the angle from the x-axis (Fig. 10). The polar coordinate system also simplifies representation of Eqs. (33) and (34):

$$M_{\text{tot}}\cos\phi_{\text{tot}} = x_{\text{tot}} = \int_{\tau} I(\tau)x(\tau)\mathrm{d}\tau \tag{39}$$

and

$$M_{\text{tot}}\sin\phi_{\text{tot}} = y_{\text{tot}} = \int_{\tau} I(\tau)y(\tau)\mathrm{d}\tau. \tag{40}$$

A vector in this x–y space can be defined as

$$\vec{r}_{\text{tot}} = \begin{bmatrix} x_{\text{tot}} \\ y_{\text{tot}} \end{bmatrix} = \int_{\tau} I(\tau)\,\vec{r}(\tau)\mathrm{d}\tau. \tag{41}$$

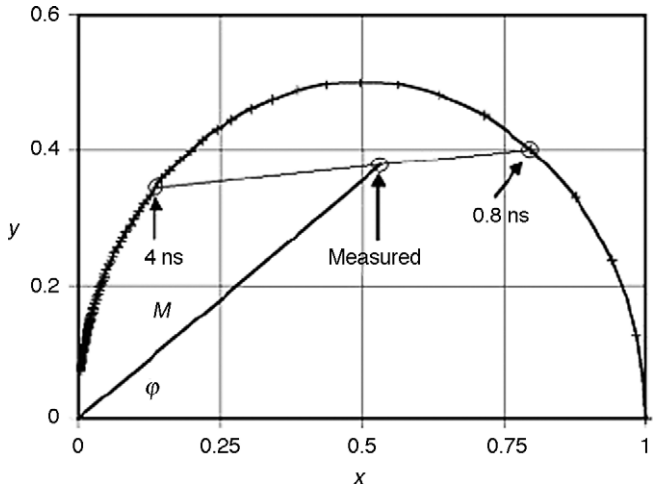

Fig. 10 A simulated plot of lifetime locations measured at 100 MHz from Redford and Clegg (2005). Axes *x* and *y* are plotted from Eqs. (37) and (38), respectively. Single lifetimes lie on the semicircle, where {1,0} represents 0 lifetime and {0,0} represents infinite lifetime. The measured value is the intensity-weighted average of the two component lifetimes. All different ratios of the two lifetime components would fall on the line between them. As illustrated in the example here, components have lifetimes of 4 and 0.8 ns (the short lifetime has two-thirds the probability/intensity of the long lifetime). The measured lifetime is phase: 1.1 and modulation: 1.8 ns. With kind permission of Springer Science and Business Media.

An advantage of this representation is that for samples with multiple lifetimes, the representation is a simple vector addition (i.e., $\vec{r}_{\text{tot}} = a\vec{r}_a + b\vec{r}_b$). Figure 10 indicates how such a plot might be constructed for a two lifetime system. For a more detailed analysis, including representation in the complex plane, see the original print in (Redford and Clegg, 2005).

IV. FLIM Techniques for Quantitative Cell Biology

A. FLIM Detection of FRET Events

FRET theory was developed by Professor Theodor Förster (Förster, 1948) and is a commonly used technique for measuring the spatial distance between two (or multiple) fluorophores. Cell biologists exploit FRET to measure the distance between two sites on a macromolecule, the distance between two proteins attached with fluorophores and hence whether and how these two proteins interact. FRET is regarded as an *in vivo* "nanoscale ruler," since it can be monitored in living cells, and the distance for FRET to occur is usually within several nanometers, exactly the distance comparable to the dimensions of biological macromolecules. The diameter of many proteins, the distance within which proteins interact in living cells, the thickness of biological membranes, and the distance between sites on multisubunit proteins are typically within this distance.

FRET mandates the presence of at least one donor–acceptor (D–A) pair, although more than one such pairs and hence distances can be involved. Readers interested in more details are referred to Chapter 15 in (Lakowicz, 1999). FRET occurs when the donor emission spectrum overlaps with the acceptor excitation spectrum. After donor excitation, energy will be transferred nonradiatively if the D–A pair is in close proximity (i.e., via the nonradiative pathway illustrated in Fig. 2 without photo emission), as a result of long-range dipole–dipole interaction between the D–A pair. In other words, the acceptor does not reabsorb the photons emitted from the donor as a means of energy transfer, which also implies that the intervening solvent or molecule has little effect on the efficiency of FRET.

How close exactly for the D–A pair will FRET occur? Quantitatively, Förster distance is defined as the distance at which the energy transfer efficiency is 50% and the energy transfer efficiency (E) is defined as

$$E = \frac{k_{\mathrm{T}}}{\tau_{\mathrm{D}}^{-1} + k_{\mathrm{T}}} \tag{42}$$

where τ_D is the donor lifetime in the absence of acceptor and k_{T} is the energy transfer rate from a donor to an acceptor. k_{T} is given by:

$$k_{\mathrm{T}} = \frac{1}{\tau_{\mathrm{D}}}\left(\frac{R_0}{r}\right)^6, \tag{43}$$

where R_0 is the Förster distance and r is the D–A distance. As we can see, when $r = R_0$, $E = 50\%$, as described in the definition of Förster distance. Also, the dependence of k_{T} on r is highly nonlinear and strong with D–A distance near R_0; when $r = 2R_0$, the energy transfer efficiency drops to only 1.56%, according to Eqs. (42) and (43).

In order to detect FRET efficiently, D–A pairs with longer R_0 are preferred. The typical value of R_0 is in the range of 20–60 Å, depending on the extent of D–A spectra overlap, the D–A orientation, the refractive index of the medium, and the quantum yield [Eq. (4)] of the donor in the absence of acceptor. Since D–A orientation is usually assumed to be dynamic and random, while refractive index of the medium typically treated as a constant for biomolecules in aqueous solution, in usual cases R_0 is considered dependent only on the optical properties of the fluorophore pairs and is approximately fixed for a given D–A pair.

To measure FRET, both steady state and time-resolved data can be used. Since k_{T} is a decay rate in addition to already existent Γ and k for donor emission decay in the absence of acceptor, the lifetime is shortened and the steady state intensity is lowered if FRET occurs. The degree of shortening/lowering is fixed if the D–A distance r is fixed, which is usually the case for labeled proteins, but in solution or membranes, where the donors and acceptors can diffuse freely, this may not be true, and calculation of an averaged k_{T} from D–A spatial distribution is required. Also, if considering multiexponential decay, which in fact happens frequently in biomolecules, an averaged τ value over all exponential curves is needed as well.

The most common application of FRET is to measure the distances between two sites on a macromolecule. FRET can be used to monitor any phenomena with changes in the D–A distance, such as conformational changes of a macromolecule, or the cleavage of a macromolecule by enzymes. In these cases, endogenous fluorophores are usually used. For instance, tryptophan (Table I) can be used as a donor, and a ligand that binds to a ligand-binding site can be an acceptor.

Exogenous fluorophores (e.g., CFP–YFP) are also used as D–A pairs in cell biology. In this case, donor and acceptor vectors are constructed with the proteins of interest, typically the proteins between which the *in vivo* interactions are unknown. The fluorophores can be attached on either the N-terminal or the C-terminal of the proteins, depending on the locations of functional domains of the proteins. The vectors are transfected into the model cells, usually the cell kinds that are easy to transfect, or related to the cells where the protein functions and interactions are of interest. Vector sizes could be a factor that affects FRET, if vectors are not transfected efficiently (Kreiss *et al.*, 1999; Ross and Hui, 1999), making the signals too weak and noisy, or if the ratio of transfected donor to acceptor is too high or too low.

FRET-FLIM combines FRET and lifetime imaging, which can be highly favored over intensity-based FRET for several reasons. For FRET with weak signals or low-energy transfer efficiency, a minute intensity artifact can lead to very high impreciseness in FRET detection. For example, if detection of FRET with energy transfer efficiency of $\sim$10% is desired, the variation in fluorescence emission intensity among and within cells might need to be controlled to be very low, and this may not be an easy task for low-signal experiments, for wide-field fluorescence microscopy, or for experiments with nonuniform transfection distribution. Using FLIM to detect FRET with $E = \sim$10% allows intensity variation to be as high as 30%, and theoretically even higher, given molecular microenvironment and later data-processing procedures not affected.

Figure 11 illustrates CFP–YFP FRET measured with a multiphoton TCSPC approach (Becker *et al.*, 2005). The experiment was performed in a human embryonic kidney cell expressing two interacting proteins labeled with CFP and YFP. Electronic timing & acquisition was controlled by a Becker and Hickl SPC-730 TCSPC module connected to a Zeiss LSM 510 NLO two-photon microscope. The detector was a Hamamatsu R3809U-50 MCP PMT. The upper left panel shows a single exponential lifetime image calculated from CFP emission data, providing a good indication of the intracellular distribution of FRET. However, a closer inspection of the fluorescence data in the individual pixels shows that the decay is double exponential (Fig. 11, upper right). A double exponential analysis of the decay data then disentangles the effects of the variable fraction of interacting proteins, indicated by the amplitude ratio a_{fast}/a_{slow}, and of the D–A distance, indicated by the lifetime ratio τ_{slow}/τ_{fast}. Lower panels of Fig. 11 show that most of the lifetime variation found in the single exponential lifetime image is due to a variable fraction of interacting donor and not to a change in the distance.

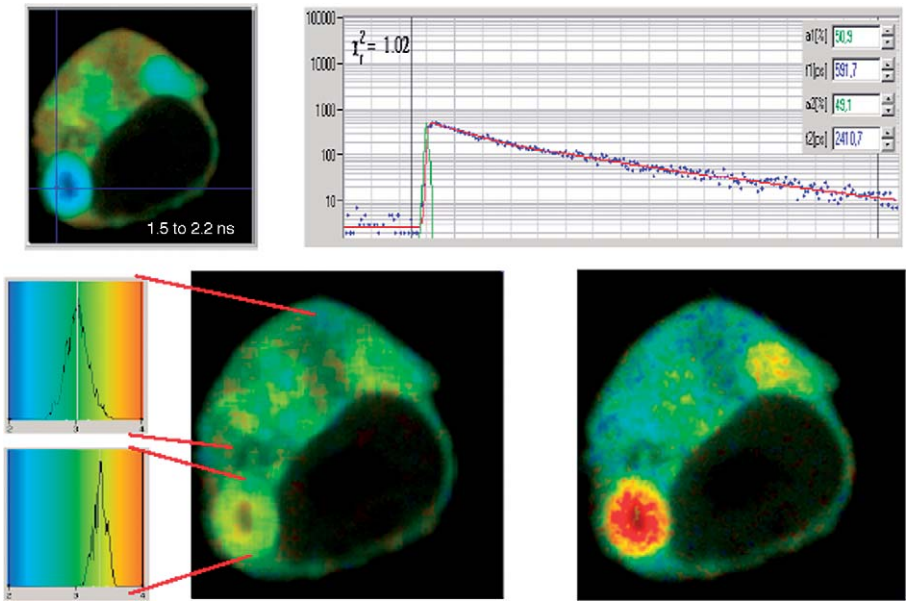

Fig. 11 Multiphoton TCSPC CFP–YFP FRET. Upper left: single exponential lifetime image, CFP channel, 480 ± 15 nm. Blue to red = 1.5–2.2 ns. Upper right: fluorescence decay in selected spot and decay components of a double exponential fit. Lower left: color represents τ_{slow}/τ_{fast}, blue to red = 2–4. The distribution of τ_{slow}/τ_{fast} is shown for an area of weak FRET (top) and strong FRET (bottom). Lower right: color represents a_{fast}/a_{slow}, blue to red = 0.2–1 (Becker *et al.*, 2005). Copyright 2004 SPIE.

In addition, a two-photon FRET-FLIM system for protein localization was characterized (Chen and Periasamy, 2004), and plasma membrane organization in cowpea protoplasts was studied using FRET-FLIM with different GFP-fused proteins (Vermeer *et al.*, 2004). An FRET-FLIM-based detection of phosphorylated protein localization, performed in FD, is shown in Fig. 1 and described in Section I (Ng *et al.*, 1999). A review on FRET-FLIM has provided a table of commonly used FRET fluorophore pairs for FLIM studies (Wallrabe and Periasamy, 2005).

B. Molecular Diffusion Rates Measured via Fluorescence Correlation Spectroscopy (FCS)-FLIM

The advent of photon counting techniques such as TCSPC has resulted in the development of statistical methods for sample analysis, broadly classified as fluorescence correlation spectroscopy (FCS). As mentioned earlier, benefits of FLIM lie in obtaining additional information than fluorophore concentration and localization; this includes the molecular environment and protein grouping and/or interactions. By measuring variations in fluorescence at a single image pixel over time, FCS provides single-point measurements of kinetic and diffusion

properties of fluorescent molecules as well as their concentration and aggregation state. The pixel volume in confocal systems is in the subfemtomolar range, and the number of fluorescent molecules in this small space will typically be one. FCS can also be used to cover dynamic phenomena on a submicrosecond time scale. FCS-FLIM provides a very useful fluorescence modality which can be implemented on confocal systems and commercial, integrated products are available for this purpose. FCS has been reported early on for studying mobility of small solutes in the cytoplasm of living cells (Berland *et al.*, 1995). Kask *et al.* (1999) used FCS for monitoring restriction enzyme-mediated cleavage of DNA hybrids by using fluorescently labeled complementary oligonucleotides. A two-channel confocal fluorescence lifetime microscope was used for FCS and FLIM, since the timing information down to a picosecond scale offered the possibility not only to reconstruct fluorescence decay of each pixel for FLIM but also to analyze the fluorescence fluctuation correlation function of any single spot of interest (Wahl *et al.*, 2004). Healthy and sorbitol-stressed cells expressing a GFP-MK2 fusion protein were studied with TCSPC and analyzed with lifetime imaging and FCS (Becker *et al.*, 2006). In stressed cells, while FLIM results demonstrated a lifetime reduction and translocation of the proteins to the cytoplasm, FCS of one single spot showed slower diffusion with higher correlation amplitude, possibly indicating aggregation of the proteins. Reviews on FCS and FLIM can also be found in (Breusegem *et al.*, 2006; Hink *et al.*, 2002).

C. Multispectral-Multiphoton-FLIM

Given the weak optical signals and high variability observable in biological samples, sensitivity is a key component of imaging studies, obtained sometimes at the cost of real-time acquisition. Complete spectral analysis of the sample is also important, especially for FRET studies where the transfer efficiency is high; if analysis is restricted to wavelength where donor fluorescence spectrum does not overlap with the acceptor fluorescence spectrum, all the information regarding acceptor fluorescence decay is lost.

Multiphoton microscopy provides high axial and lateral resolution and is optimal for deep tissue imaging. TCSPC can be used to provide lifetime-resolved images with a resolution of 30 ps (Becker *et al.*, 2002), and a multichannel TCSPC module coupled to a parallel PMT system can provide spectral resolution (Becker *et al.*, 2004). Such a system provides high spatial, temporal, and satisfactory spectral resolution and is termed as multispectral-multiphoton-FLIM (MS-MP-FLIM). Disadvantages include long acquisition times, which can be on the order of tens of minutes. The spectral and temporal resolution of MS-MP-FLIM can be further enhanced (at a significant cost) by employing a device called a streak camera (Fig. 12). It has been demonstrated that with a streak camera, 6 ps temporal resolution can be achieved and spectral resolution is considerably improved (1–3 nm), since a spectrograph is used to focus the signal into the entrance slit of a streak camera (Qu *et al.*, 2006).

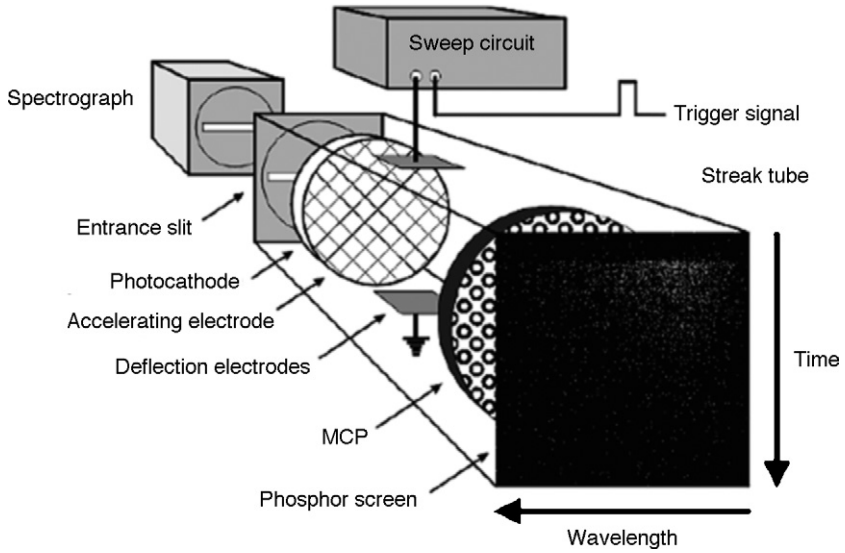

Fig. 12 Design of a streak camera. A CCD camera after the MCP (not shown here) provides a 2D plot of wavelength versus delay (see text for full details) (Biskup *et al.*, 2005). Copyright 2005 SPIE.

Inside the streak camera, the signal is converted to photoelectrons via a photocathode and accelerated by an electrode. A pair of deflection electrodes is used to apply a ramp voltage that sweeps the electrons from top to bottom, with electrons that arrive earlier leaving near the top, and vice versa. Hence, the vertical position of the photoelectron is a function of delay. The signal is amplified via a microchannel plate (MCP) and reconverted into an optical signal at a phosphor screen. A CCD camera placed after the phosphor screen is used for digital imaging of the streak image, which contains temporal distribution of intensity as a function of wavelength. Streak images can be used to regenerate the spectrum as well as the fluorescence decay curve. Figure 13 illustrates the high spatial and temporal resolution possible with streak camera systems, with a narrow lifetime distribution around the mean (Biskup *et al.*, 2005).

D. Video-Rate FLIM for Single-Shot Lifetime Image Acquisition

While scanning techniques such as multiphoton FLIM provide a faculty for high resolution imaging, they are inadequate for studying dynamic phenomena, such as fluid mixing in microfluidic channels. Wide-field microscopy, with parallel pixel capture and single-shot imaging capability, provides a better scenario for implementing high frame rate imaging (>1 frame/s). Several flavors of video-rate FLIM can be found, from heterodyne-based frequency domain to time domain, from endoscopic FLIM to *in vitro* studies (Elson *et al.*, 2004; Munro *et al.*, 2005; Siegel *et al.*, 2003).

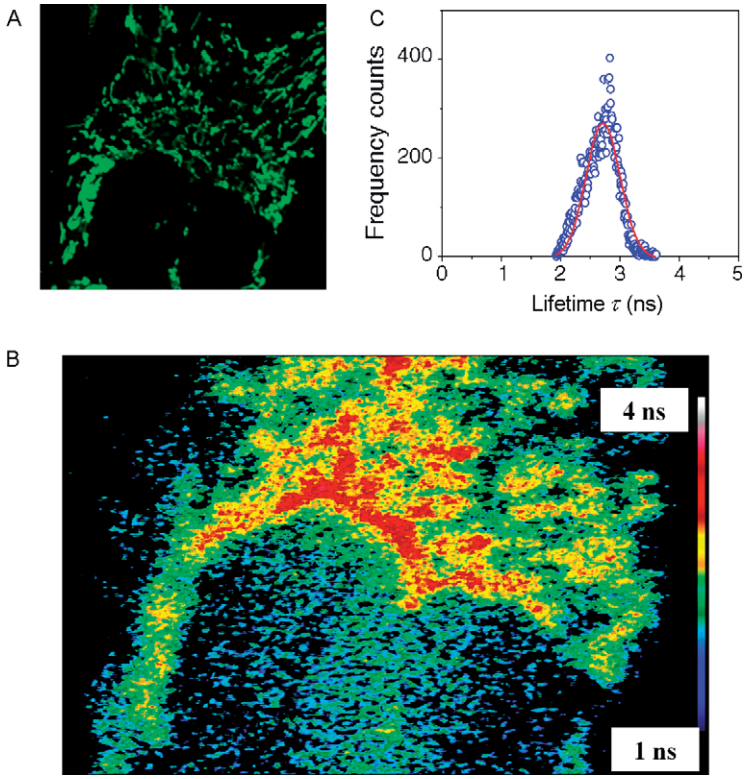

Fig. 13 Multiphoton image (A), streak FLIM image (B), and lifetime histogram (C) of a baby hamster kidney (BHK) cell transfected with mitochondria-targeted enhanced cyan fluorescent proteins (mECFP). Lifetime value inside the mitochondria is 2.71 ± 0.25 ns. Reused with permission from Krishnan *et al.* (2003). Copyright 2003, American Institute of Physics.

Elson *et al.* (2004) reported two different time-domain approaches implemented on the same FLIM system to achieve video-rate (29 fps) capability. Both involve modifications to a conventional wide-field FLIM system, which has been described elsewhere (Cole *et al.*, 2001). The first approach involves the use of a rapid delay generator that can vary the electronic delay to the gated imager in 2 ms. Two images are acquired and evaluated using the RLD algorithm. Lifetimes can be measured in the range of 120 ps to 4 ns with a discrimination of 100 ps. The limitation in lifetime measurement is due to the use of a high repetition laser, which can potentially be circumvented by the use of a low repetition source such as a nitrogen-pumped dye laser (Urayama *et al.*, 2003).

Another technique called single-shot FLIM was presented to circumvent the sequential image capture process that is characteristic of TD FLIM. The design arises from the possibility that if the same emission signal can be split two or more ways and each one be gated differently, the lifetime can be reconstructed from a

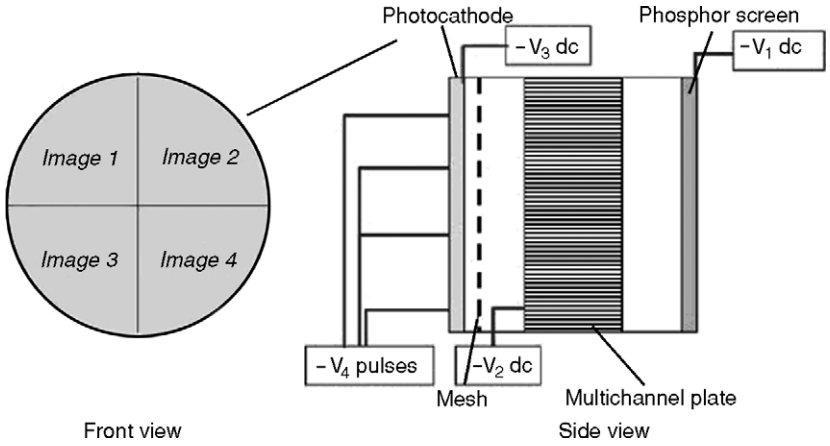

Fig. 14 Schematic representation of a segmented GOI system. Gating is switched by controlling cathode to multichannel plate voltage (V_4,V_3) and gain is established via V_2. The four-gate GOI is capable of gates in the range 100 ps to 5 ns, 10 μs to 1ms and DC operation (Elson *et al.*, 2004). Copyright 2004 IOP Publishing Limited.

single emission response. The segmented GOI (Kentech instruments) has four quadrants which can be independently gated, though by design all gates must have the same duration (Fig. 14). A commercially available four-channel optical intensity splitter is used to relay four images of the sample onto the SGOI. On imaging on the CCD, the corresponding pixels in each of the subimages can be analyzed for lifetime, a process easily done with image-processing software.

V. Summary

In this chapter, the basic concepts, key advantages, and several applications of FLIM have been discussed. Continuing advances in technology for microscopy and the developing appreciation that fluorescence lifetime is a sensitive means for evaluating microenvironment will likely help make FLIM a critical research tool for cell biology by providing a new way for cell biologists to detect, visualize, and investigate structure and function in biological systems.

Acknowledgments

This work was supported in part by the National Institutes of Health grant CA-112173 (to M.-A.M.).

References

Becker, W. (2005). "Advanced Time-Correlated Single Photon Counting Techniques." Springer-Verlag, Berlin, Heidelberg.

Becker, W., and Bergmann, A. (2003). Lifetime imaging techniques for optical microscopy. http://www.boselec.com/products/documents/TCSPCformicroscopy12-29-04.pdf

Becker, W., Bergmann, A., Haustein, E., Petrasek, Z., Schwille, P., Biskup, C., Anhut, T., Riemann, I., and Koenig, K. (2005). Fluorescence lifetime images and correlation spectra obtained by multidimensional TCSPC. *Proc. SPIE* **5700,** 144–151.

Becker, W., Bergmann, A., Hink, M. A., Konig, K., Benndorf, K., and Biskup, C. (2004). Fluorescence lifetime imaging by time-correlated single-photon counting. *Microsc. Res. Tech.* **63**(1), 58–66.

Becker, W., Bergmann, A., Haustein, E., Petrasek, Z., Schwille, P., Biskup, C., Kelbauskas, L., Benndorf, K., Klocker, N., Anhut, T., Riemann, I., and Konig, K. (2006). Fluorescence lifetime images and correlation spectra obtained by multidimensional time-correlated single photon counting. *Microsc. Res. Tech.* **69**(3), 186–195.

Becker, W., Bergmann, A., and Weiss, G. (2002). Lifetime imaging with the Zeiss LSM-510. *Proc. SPIE* **4620,** 30–35.

Berland, K. M., So, P. T. C., and Gratton, E. (1995). Two-photon fluorescence correlation spectroscopy—method and application to the intracellular environment. *Biophys. J.* **68**(2), 694–701.

Biskup, C., Kelbauskas, L., Zimmer, T., Dietrich, S., Benndorf, K., Becker, W., Bergmann, A., and Klöcker, N. (2005). Spectrally resolved fluorescence lifetime and FRET measurements. *Proc. SPIE* **5700,** 188–196.

Böhmer, M., Pampaloni, F., Wahl, M., Rahn, H.-J., Erdmann, R., and Enderlein, J. (2001). Time-resolved confocal scanning device for ultrasensitive fluorescence detection. *Rev. Sci. Instrum.* **72**(11), 4145–4152.

Booth, M. J., and Wilson, T. (2004). Low-cost, frequency-domain, fluorescence lifetime confocal microscopy. *J. Microsc.* **214**(Pt. 1), 36–42.

Breusegem, S. Y., Levi, M., and Barry, N. P. (2006). Fluorescence correlation spectroscopy and fluorescence lifetime imaging microscopy. *Nephron Exp. Nephrol.* **103**(2), e41–e49.

Bugiel, I., König, K., and Wabnitz, H. (1989). Investigation of cell by fluorescence laser scanning microscopy with subnanosecond time resolution. *Laser Life Sci.* **3**(1), 47–53.

Chen, Y., and Periasamy, A. (2004). Characterization of two-photon excitation fluorescence lifetime imaging microscopy for protein localization. *Microsc. Res. Tech.* **63**(1), 72–80.

Cole, M. J., Siegel, J., Webb, S. E. D., Jones, R., Dowling, K., Dayel, M. J., Parsons-Karavassilis, D., French, P. M. W., Lever, M. J., Sucharov, L. O. D., Neil, M. A. A., Juskaitis, R., *et al.* (2001). Time-domain whole-field fluorescence lifetime imaging with optical sectioning. *J. Microsc.* **203**(3), 246–257.

Cubeddu, R., Comelli, D., D'Andrea, C., Taroni, P., and Valentini, G. (2002). Time-resolved fluorescence imaging in biology and medicine. *J. Phys. D Appl. Phys.* **35,** R61–R76.

Demas, J. N. (1983). ''Excited State Lifetime Measurements.'' Academic Press, New York.

Dowling, K., Hyde, S. C. W., Dainty, J. C., French, P. M. W., and Hares, J. D. (1997). 2-D fluorescence lifetime imaging using a time-gated image intensifier. *Opt. Commun.* **135,** 27–31.

Elson, D. S., Munro, I., Requejo-Isidro, J., McGinty, J., Dunsby, C., Galletly, N., Stamp, G. W., Neil, M. A. A., Lever, M. J., Kellett, P. A., Dymoke-Bradshaw, A., Hares, J., *et al.* (2004). Real-time time-domain fluorescence lifetime imaging including single-shot acquisition with a segmented optical image intensifier. *New J. Phys.* **6,** 1–13.

Förster, T. (1948). Intermolecular energy migration and fluorescence. *Ann. Phys. (Leitzig)* **2,** 55–75.

French, T., So, P. T. C., Dong, C. Y., Berland, K. M., and Gratton, E. (1998). Fluorescence lifetime imaging techniques for microscopy. *Methods Cell Biol.* **56,** 277–304.

Gadella, T. W. J., Jr. (1999). Fluorescence lifetime imaging microscopy (FLIM): Instrumentation and application. *In* ''Fluorescent and Luminescent Probes for Biological Activity'' (W. T. Masons, ed.), pp. 467–479. Academic Press, San Diego.

Gerritsen, H. C., Sanders, R., Draaijer, A., and Levine, Y. K. (1997). Fluorescence lifetime imaging of oxygen in living cells. *J. Fluoresc.* **7,** 11–16.

Ghiggino, K. P., Harris, M. R., and Spizzirri, P. G. (1992). Fluorescence lifetime measurements using a novel fiber-optic laser scanning confocal microscope. *Rev. Sci. Instrum.* **63**(5), 2999–3002.

Hink, M. A., Bisselin, T., and Visser, A. J. (2002). Imaging protein-protein interactions in living cells. *Plant Mol. Biol.* **50**(6), 871–883.

ISS. Lifetime data of selected fluorophores. http://www.iss.com/resources/fluorophores.html

Kask, P., Palo, K., Ullmann, D., and Gall, K. (1999). Fluorescence-intensity distribution analysis and its application in biomolecular detection technology. *Proc. Natl. Acad. Sci. USA* **96**(24), 13756–13761.

Kreiss, P., Cameron, B., Rangara, R., Mailhe, P., Aguerre-Charriol, O., Airiau, M., Scherman, D., Crouzet, J., and Pitard, B. (1999). Plasmid DNA size does not affect the physicochemical properties of lipoplexes but modulates gene transfer efficiency. *Nucleic Acids Res.* **27**(19), 3792–3798.

Krishnan, R. V., Saitoh, H., Terada, H., Centonze, V. E., and Herman, B. (2003). Development of a multiphoton fluorescence lifetime imaging microscopy system using a streak camera. *Rev. Sci. Instrum.* **74**(5), 2714–2721.

Lakowicz, J. R. (1999). "Principles of Fluorescence Spectroscopy." Kluwer Academic/Plenum, New York.

Lakowicz, J. R., Szmacinski, H., Nowaczyk, K., and Johnson, M. L. (1992). Fluorescence lifetime imaging of free and protein-bound NADH. *Proc. Natl. Acad. Sci. USA* **89**(4), 1271–1275.

Lee, K. C. B., Siegel, J., Webb, S. E. D., Leveque-Fort, S., Cole, M. J., Jones, R., Dowling, K., Lever, M. J., and French, P. M. W. (2001). Application of the stretched exponential function to fluorescence lifetime imaging. *Biophys. J.* **81,** 1265–1274.

Lin, H. J., Herman, P., and Lakowicz, J. R. (2003). Fluorescence lifetime-resolved pH imaging of living cells. *Cytometry A* **52**(2), 77–89.

Munro, I., McGinty, J., Galletly, N., Requejo-Isidro, J., Lanigan, P. M. P., Elson, D. S., Dunsby, C., Neil, M. A., Lever, M. J., Stamp, G. W., and French, P. M. (2005). Toward the clinical application of time-domain fluorescence lifetime imaging. *J. Biomed. Opt.* **10**(5), 051403.

Ng, T., Squire, A., Hansra, G., Bornancin, F., Prevostel, C., Hanby, A., Harris, W., Barnes, D., Schmidt, S., Mellor, H., Bastiaens, P. I. H., and Parker, P. J. (1999). Imaging protein kinase C alpha activation in cells. *Science* **283**(5410), 2085–2089.

Oida, T., Sako, Y., and Kusumi, A. (1993). Fluorescence lifetime imaging microscopy (flimscopy)—methodology development and application to studies of endosome fusion in single cells. *Biophys. J.* **64**(3), 676–685.

Qu, J. L., Liu, L. X., Chen, D. N., Lin, Z. Y., Xu, G. X., Guo, B. P., and Niu, H. B. (2006). Temporally and spectrally resolved sampling imaging with a specially designed streak camera. *Opt. Lett.* **31**(3), 368–370.

Redford, G. I., and Clegg, R. M. (2005). Polar plot representation for frequency-domain analysis of fluorescence lifetimes. *J. Fluoresc.* **15**(5), 805–815.

Ross, P. C., and Hui, S. W. (1999). Lipoplex size is a major determinant of *in vitro* lipofection efficiency. *Gene Ther.* **6**(4), 651–659.

Rudolph, W., and Kempe, M. (1997). Trends in optical biomedical imaging. *J. Mod. Opt.* **44**(9), 1617–1642.

Salthammer, T. (1992). Numerical simulation of pile-up distorted time-correlated single photon counting (TCSPC) data. *J. Fluoresc.* **2**(1), 23–27.

Sanders, R., Draaijer, A., Gerritsen, H. C., Houpt, P. M., and Levine, Y. K. (1995). Quantitative pH imaging in cells using confocal fluorescence lifetime imaging microscopy. *Anal. Biochem.* **227**(2), 302–308.

Sharman, K. K., Periasamy, A., Ashworth, H., Demas, J. N., and Snow, N. H. (1999). Error analysis of the rapid lifetime determination method for double-exponential decays and new windowing schemes. *Anal. Chem.* **71**(5), 947–952.

Siegel, J., Elson, D. S., Webb, S. E. D., Lee, K. C. B., Vlanclas, A., Gambaruto, G. L., Leveque-Fort, S., Lever, M. J., Tadrous, P. J., Stamp, G. W. H., Wallace, A. L., Sandison, A., *et al.* (2003). Studying biological tissue with fluorescence lifetime imaging: Microscopy, endoscopy, and complex decay profiles. *Appl. Opt.* **42**(16), 2995–3004.

Sud, D., Zhong, W., Beer, D. G., and Mycek, M.-A. (2006). Time-resolved optical imaging provides a molecular snapshot of altered metabolic function in living human cancer cell models. *Opt. Express* **14**(10), 4412–4426.

Tadrous, P. J. (2000). Methods for imaging the structure and function of living tissues and cells: 2. Fluorescence lifetime imaging. *J. Pathol.* **191**(3), 229–234.

Urayama, P. K., and Mycek, M.-A. (2003). Fluorescence lifetime imaging microscopy of endogenous biological fluorescence. *In* "Handbook of Biomedical Fluorescence" (M.-A. Mycek, and B. W. Pogue, eds.), pp. 211–236. Marcel Dekker, Inc., New York.

Urayama, P. K., Zhong, W., Beamish, J. A., Minn, F. K., Sloboda, R. D., Dragnev, K. H., Dmitrovsky, E., and Mycek, M.-A. (2003). A UV-visible fluorescence lifetime imaging microscope for laser-based biological sensing with picosecond resolution. *Appl. Phys. B-Lasers Opt.* **76**(5), 483–496.

Vermeer, J. E., Van Munster, E. B., Vischer, N. O., and Gadella, T. W., Jr. (2004). Probing plasma membrane microdomains in cowpea protoplasts using lipidated GFP-fusion proteins and multimode FRET microscopy. *J. Microsc.* **214**(Pt. 2), 190–200.

Wahl, M., Koberling, F., Patting, M., Rahn, H., and Erdmann, R. (2004). Time-resolved confocal fluorescence imaging and spectrocopy system with single molecule sensitivity and sub-micrometer resolution. *Curr. Pharm. Biotechnol.* **5**(3), 299–308.

Wallrabe, H., and Periasamy, A. (2005). Imaging protein molecules using FRET and FLIM microscopy. *Curr. Opin. Biotechnol.* **16**(1), 19–27.

Wang, X. F., Periasamy, A., Herman, B., and Coleman, D. (1992). Fluorescence lifetime imaging microscopy (FLIM): Instrumentation and applications. *Crit. Rev. Anal. Chem.* **23**(5), 369–395.

Wang, X. F., Uchida, T., Coleman, D. M., and Minami, S. (1991). A two-dimensional fluorescence lifetime imaging system using a gated image intensifier. *Appl. Spectrosc.* **45**(3), 360–366.